Marine and Petroleum Geology 89 (2018) 14–26

Contents lists available at ScienceDirect

Marine and Petroleum Geology

journal homepage: www.elsevier.com/locate/marpetgeo

Research paper

Pore characterization of Lower Silurian shale gas reservoirs in the Middle Yangtze region, central China

Qingtao Wang [a], Hong Lu [a, *], Taoli Wang [a, b], Dayong Liu [a], Ping'an Peng [a], Xin Zhan [c], Xianqing Li [d, e]

[a] State Key Laboratory of Organic Geochemistry, Guangzhou Institute of Geochemistry, Chinese Academy of Sciences, Guangzhou 510640, PR China
[b] University of Chinese Academy of Sciences, Beijing, 100049, PR China
[c] Geology and Geophysics Program, Missouri University of Sciences and Technology, Rolla, MO 65409, USA
[d] State Key Laboratory of Coal Resources and Safe Mining, China University of Mining and Technology (Beijing), Beijing 100083, PR China
[e] College of Geoscience and Surveying Engineering, China University of Mining and Technology (Beijing), Beijing 100083, PR China

ARTICLE INFO

Article history:
Received 12 July 2016
Received in revised form
15 December 2016
Accepted 19 December 2016
Available online 21 December 2016

Keywords:
Shale gas
Pore structure
Organo-clay complex
Longmaxi shale

ABSTRACT

Organic-rich shales from Lower Silurian are widely distributed in the Middle Yangtze region, central China. However, the lack of fundamental data for shale gas reservoirs increases the difficulty of gas exploration. In this study, 34 core samples were collected to characterize the shale pore structure and conduct a preliminary evaluation of the shale gas reservoir. The TOC (total organic carbon) content of the successively-deposited black shales range from 1.6% to 5.9%, while the total porosity range from 0.5% to 4.2%. The positive correlation between TOC and porosity indicates that TOC is the key factor determining porosity. The major component of the mineral matrix is quartz (content of 21.4%–69.2%), followed by clay minerals (content of 16.7%–44.5%). Field-emission scanning electron microscopy (FE-SEM) and energy dispersive X-ray spectroscopy (EDS) results illustrate that organic matter, mixed with clay minerals, can form an organo-clay complex containing many nanopores. Furthermore, larger organic pores are developed in organo-clay complexes with higher clay content than in those with lower clay content.

Correlational analyses between pore volume (or pore surface area) and TOC (or clay content) demonstrate that micropores are associated with organic matter, while mesopores and macropores are probably associated with clay minerals. Many of the clay-related nanopores are organic in nature and are developed in organo-clay complexes containing both organic matter and clay minerals. Overall, the TOC content controls development of nanopores in the shale pore structure, followed by clay content. The DFT-derived PSD indicates that the pore volume is comprised primarily of pores having widths larger than 10 nm, while the surface area is comprised primarily of micropores. When considering the gas in place model and mechanisms of shale gas storage, further shale gas exploration in central China should aim to the deep (>1000 m) and well preserved Longmaxi Shales.

1. Introduction

Given the improvements in drilling and completion technology, large quantities of natural gas can now be produced from organic-rich shales of low permeability (Curtis, 2002; King et al., 2015; Montgomery et al., 2005). Shale gas exploration has received renewed attention in United States of America (Curtis et al., 2012; Hao and Zou, 2013; Loucks et al., 2012; Loucks and Ruppel, 2007), Canada (Chalmers et al., 2012a; Ross and Marc Bustin, 2009), Germany (Bernard et al., 2012) and China (Tian et al., 2013, 2015; Zou et al., 2010). These shales not only serve as the gas reservoir, but also as the source, trap, and seal for the gas (Chalmers et al., 2012a; Tian et al., 2013). The shale gas is either stored in large pores and microfractures as free gas, or absorbed on the surface of kerogen and clay aggregate (Chalmers et al., 2012a; Curtis, 2002). In contrast to conventional sandstone and carbonate reservoirs, very small pores exist in shales, ranging from several to hundreds of nanometers (Loucks et al., 2012; Ross and Marc Bustin, 2009). Research of nanopore networks takes priority because the type, size, and arrangement of pores significantly affects the storage, transport

* Corresponding author. Room 636, Biaoben Building, NO. 511 Kehua Street, Wushan, Tianhe District, Guangzhou City, Guangdong Province, PR China.
E-mail address: luhong@gig.ac.cn (H. Lu).

http://dx.doi.org/10.1016/j.marpetgeo.2016.12.015
0264-8172/

(King et al., 2015; Ross and Marc Bustin, 2009) and volume of potential shale gas reserves.

Various techniques have been borrowed from material science to illustrate the complexity of pore networks in shales. Total porosity can be determined by helium pycnometry and mercury porosimetry (Chalmers et al., 2012a; Eseme et al., 2006; Ross and Marc Bustin, 2009), while surface area and pore size distribution can be calculated from N_2/CO_2 adsorption (Tian et al., 2013, 2015; Wang et al., 2015), mercury injection capillary pressure (Cao et al., 2015; Ma et al., 2015; Ross and Marc Bustin, 2009; Wang et al., 2014), along with small/ultra-small angle neutron scattering (King et al., 2015; Mastalerz et al., 2012; Ruppert et al., 2013). Moreover, field emission scanning electron microscopy (FE-SEM), transmission electron microscopy (TEM) and helium ion microscopy provide high-resolution (~5 nm) images which make it possible to observe nanopore geometries in shales (King et al., 2015). Loucks et al. (2012) classified individual nanopores into one of four groups: intra- and inter-pores within minerals, pores in organic matter (OM) and microfractures (Loucks et al., 2012). Organic pores are regarded as a significant component of the pore system in shales (Curtis, 2002; Löhr et al., 2015; Loucks et al., 2012; Milliken et al., 2013; Ross and Marc Bustin, 2009), as demonstrated by the positive relationship between total porosity and TOC content (Milliken et al., 2012, 2013; Tian et al., 2015). The fine-grained mineral matrix also influences the size, distribution and arrangement of pore spaces as evidenced by the large amounts of microporosity found in clay platelets (Ross and Marc Bustin, 2009; Wang et al., 2014) or in the organo-clay complex (Wang et al., 2014). Although our knowledge of the pore network in shales is evolving, a deeper understanding of gas storage mechanisms is required to better assess the economic feasibility of, and to reduce the risks of gas exploration (King et al., 2015; Ross and Marc Bustin, 2009).

Most shale gas exploration in China is conducted in the south part of the country where thick marine shales are widely distributed. Four shale formations are regarded as targets: the Doushantuo Shale Formation of Late Sinian age, the Niutitang/Qingzhusi Shale of Early Cambrian age, the Longmaxi Shale of Early Silurian age, and the Dalong/Longtan/Gufeng Shale of Late Permian age (Tian et al., 2015; Wang et al., 2015; Zou et al., 2010). Until now, large volumes of shale gas have been acquired from the Lower Silurian Longmaxi Formation in the Sichuan Basin in SW China.

The Middle Yangtze region (Fig. 1) is adjacent to the key gas-producing area and the Longmaxi Shale in this area is widely distributed with high TOC and brittle mineral content (Qiu et al., 2013). Numerous companies and organizations, including Petrochina, Sinopec, China Huadian Corporation and China Geological Survey (Wuhan center), have explored the Middle Yangtze region. However, the lack of research in characterizing the pore networks of shale gas reservoirs raises the risk in gas exploration (Wang et al., 2015).

Given that pore structure and porosity are closely related to the gas sorption process and total gas capacity (Ross and Marc Bustin, 2009), this study was designed to characterize the porosity, pore surface area and pore size distribution of gas-bearing shales, and how these parameters were influenced by both organic (TOC) and inorganic (e.g. clay) content. Moreover, many researchers emphasize that commercial shale gas fields are almost closed system and have sufficient gas remained in shales. (Guo and Zhang, 2014; Hao et al., 2013). This research in pore structure for shale gas reservoirs provides new insight into the existing model of shale gas storage.

2. Geologic settings

The Middle Yangtze region covers an area of about 14×10^4 km^2 and is comprised of regions in Hubei province, the northwest part of Hunan province and the east part of Chongqing City. It is bounded by the Qingfeng-Xiangguang fault to the north, by the Jianshi-Pengshui fault to the west, and by the Jiangnan fault to the southeast (Qiu et al., 2013) (Fig. 1). This area subsided continuously during the Cambrian before being slowly uplifted from the Middle Ordovician to the Late Silurian. In response to tectonic movement, the depositional environment of the Middle Yangtze region varied from a shallow shelf to a shallow water carbonate platform and then back to a shallow shelf (Writing group for Petroleum Geology in Sichuan area, 1989). As a result, a set of black siliceous shales—the Late Ordovician Wufeng Shale and the Early Silurian Longmaxi Shale—were deposited. The Longmaxi Formation consists of three sections: (1) the lower section dominated by organic and silicious-rich black shales with abundant graptolite fossils; (2) the middle section of black and gray interbedded shale; and (3) the upper section of thick gray shale with a few thin black shale interlayers. The stratigraphic column is shown in Fig. 2. The total thickness of the Wufeng and Longmaxi Shales can exceed one hundred meters with TOC contents ranging from 0.5% to 2.38% (Qiu et al., 2013). The organic matter in these black shales are mainly during the gas window stage with equivalent vitrinite reflectance values ranging from 1.5% to 2.5% (Qiu et al., 2013), and the kerogen is dominated by type I & II (Tian et al., 2013; Zou et al., 2010).

3. Samples and experiments

3.1. Samples

A shallow well was drilled to evaluate the Longmaxi Shale gas reservoir in Huanghua country of Yichang City (YH well) (Fig. 1). Thirty-four core samples were collected from the YH well, covering the entire Wufeng and Longmaxi formations. As show in Fig. 2, both Wufeng and Lower Longmaxi formations consist of black shales with abundant graptolite fossils. The colours of shales lighten upward through the geologic column with gray interbeds in the middle and pure gray shale in upper part of the Longmaxi Formation.

3.2. Organic geochemistry, petrology and helium porosity

The total organic carbon (TOC) of the samples was determined by a LECO CS-200 analyzer following removal of carbonates by HCl digestion.

X-ray diffraction (XRD) analysis was conducted on the samples using a Bruker D8 Advance X-ray diffracto-meter at 40 kV and 30 mA with a Cu Kα radiation ($\lambda = 1.5406$ for CuKα1). Stepwise scanning measurements were performed at a rate of 4°/min in the range of 3° to 85°(2θ). Results were analyzed using XPower software to provide semi-quantitative measurements of mineral compositions.

The total porosity of the samples can be determined by the difference between the bulk density and grain density (Chalmers et al., 2012a; Tian et al., 2013). The grain density of a 1-inch diameter cylindrical shale block was measured by helium pycnometry following overnight drying at 110 °C in a vacuum oven. The bulk density was measured by first weighing the shale block in the air before and after paraffin coating ($\rho = 0.9$ cm^3/g). The coated sample was then weighed in water to calculate its total volume (shale plus paraffin). Thus, the volume of the shale block equals the difference between the total volume and paraffin volume. Subsequently, the bulk density can be obtained from the relationship between its weight and volume.

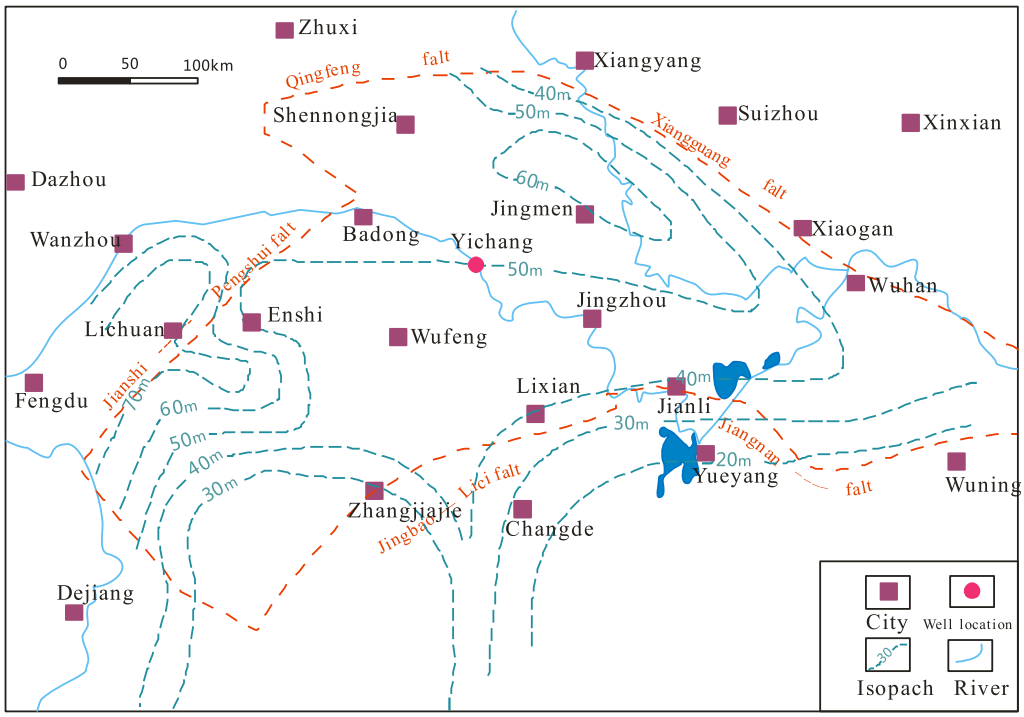

Fig. 1. Tectonic structure and the isopachs of organic-rich Longmaxi Shale in the Middle Yangtze region (modified from Qiu et al., 2013).

3.3. Low pressure N_2 and CO_2 adsorption

Low pressure N_2 and CO_2 adsorption measurements have been widely applied to characterize the nanopores in shales (Chalmers et al., 2012a; Chen and Xiao, 2014; Ross and Marc Bustin, 2009; Tian et al., 2015). For this study, N_2 and CO_2 adsorption experiments were conducted using a ASAP 2020M (Micromeritics Instruments). The shale samples were first crushed into 60–120 mesh grains (Chen et al., 2015) and then dried overnight in a vacuum oven at 110 °C to remove the residual water and other gases. Low pressure N_2 adsorption was obtained at 77 K with relative pressures ranging from 0.005 to 0.995. The equivalent surface area was calculated using the BET (Brunauer–Emmett–Teller) equation (Brunauer et al., 1938), while mesopore and macropore volumes were calculated using the BJH equation (Barrett et al., 1951) assuming a cylindrical pore. CO_2 adsorption was conducted at 273 K with relative pressures ranging from 0.00001 to 0.032 (Ghosal and Smith, 1996). The surface area and volume of the micropores were calculated by the density functional theory (DFT) equation (Wang et al., 2014).

3.4. Field emission scanning electron microscopy (FE-SEM) imaging and energy dispersive X-ray spectroscopy (EDS) analysis

Small shale blocks (1 cm by 0.5 cm by 0.5 cm) were polished by Ar ion milling (IM4000, Hitachi High-Tech) with an accelerating voltage of 3 KV and a milling time of 2 h. The images were obtained on the Hitachi S8010 system associated with the EDS microprobe. These images vividly display the nanopore in shales, which helps to identify the pore types, location and connectivity (Loucks et al., 2012). EDS measurements were made to obtain elemental composition using an accelerating voltage of 15 KV and a resolution ratio of 130.2 eV.

4. Results and discussions

4.1. Organic geochemistry and mineral compositions

The TOC content of the 34 shale samples varies from 0.13% to 5.9% and increases with depth (Fig. 3 a). The highest TOC value occurs near the bottom of the Longmaxi Formation and then decreases (yet remains relatively high) at the top of the Wufeng Formation. This pattern is indicative of the dominant nature of the organic-rich shales deposited in these parts of the two formations. Shale gas deposits in China which are technically and economically viable for extraction are mainly located in the upper Yangtze region. However, the richness of organic matter in the Longmaxi and Wufeng formations in this region is slightly higher than that in the upper Yangtze region (Guo and Zhang, 2014; Tian et al., 2013). The organic matter is thought to be composed of maceral assemblages (Ross and Marc Bustin, 2009) and pyrobitumen (Bernard et al., 2012; Mastalerz et al., 2012), which are related with organic matter conversion and oil cracking, respectively.

As shown by data in the supplementary file, the mineral compositions of most shale samples are dominated by quartz (21.4%–69.2%) but also contain large quantities of clay (16.7%–44.5%). Illite (11.3%–33.3%) dominates the clay fraction while chlorite compositions range from 5.3% to 17.6%. No kaolinite was detected. The clay content in shales collected decreases with depth in the Longmaxi Formation but increases with depth in the Wufeng Formation (Fig. 3 b). High clay content may reduce the effectiveness of hydraulic fracturing. Nevertheless, the availability of sufficient amounts of quartz may counteract this effect and maintain brittleness for fracturing (De Silva et al., 2015). Shales rich in both TOC and quartz are usually targeted for exploration because such shales have high potential to produce and store methane within organic matter, as well as being suitable for hydraulic fracturing (Chalmers et al., 2012b). The content of quartz having a biogenic origin correlates with TOC content as described for the British Columbia

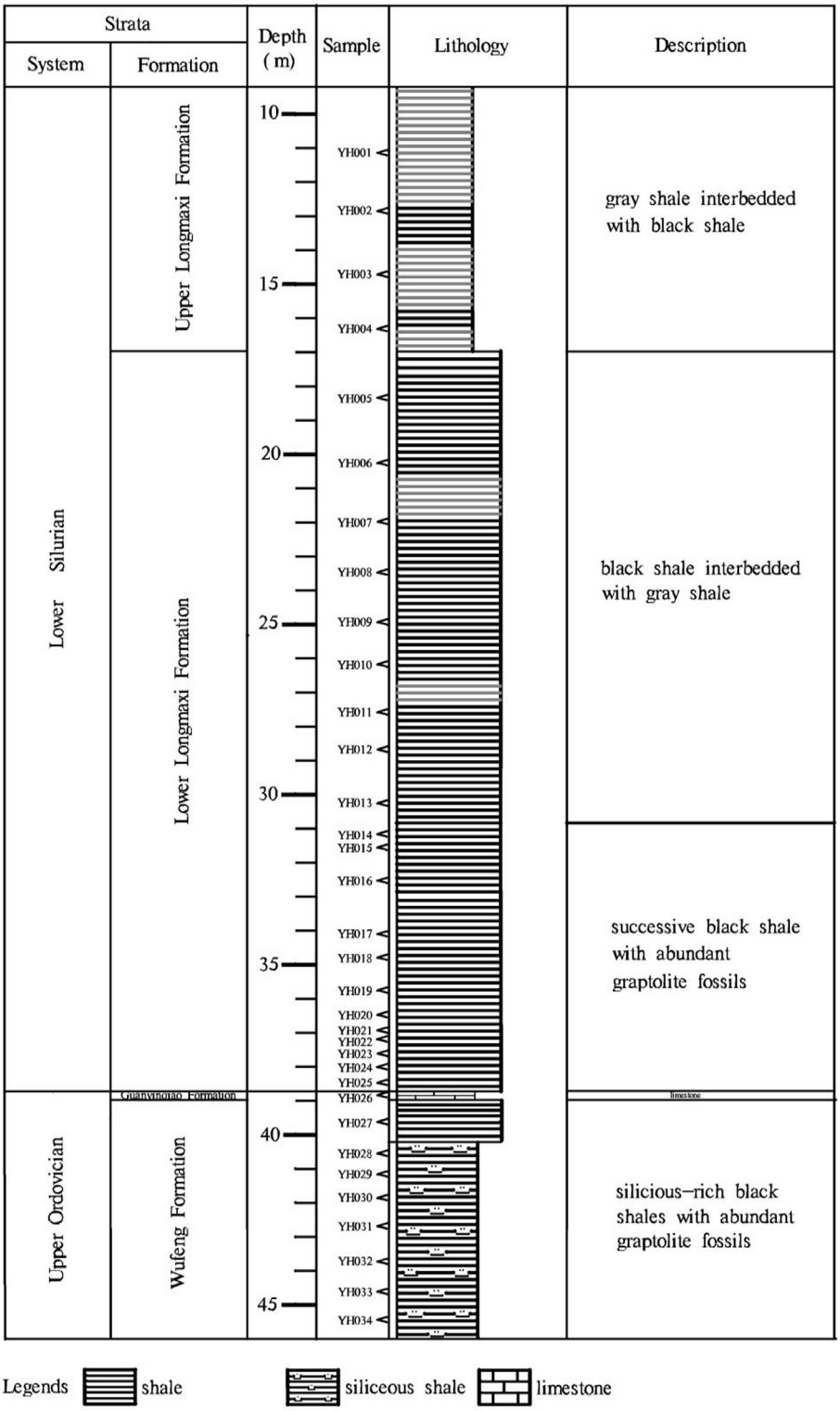

Fig. 2. Stratigraphic column showing black shales from Lower Silurian and Upper Ordovician.

Devonian gas shale (Chalmers et al., 2012b). Nevertheless, no obvious correlations between quartz and TOC contents were found in this study, probably due to insufficient amounts of biogenic quartz in the tested samples. While the majority of samples had low carbonate contents, averaging about 5%, a few had contents of greater than 10%. Samples with the higher contents likely contained part of a thin carbonate vein filling in micro fractures. Albite and pyrite contents ranged from 8.5% to 23.1% and less than 5%, respectively.

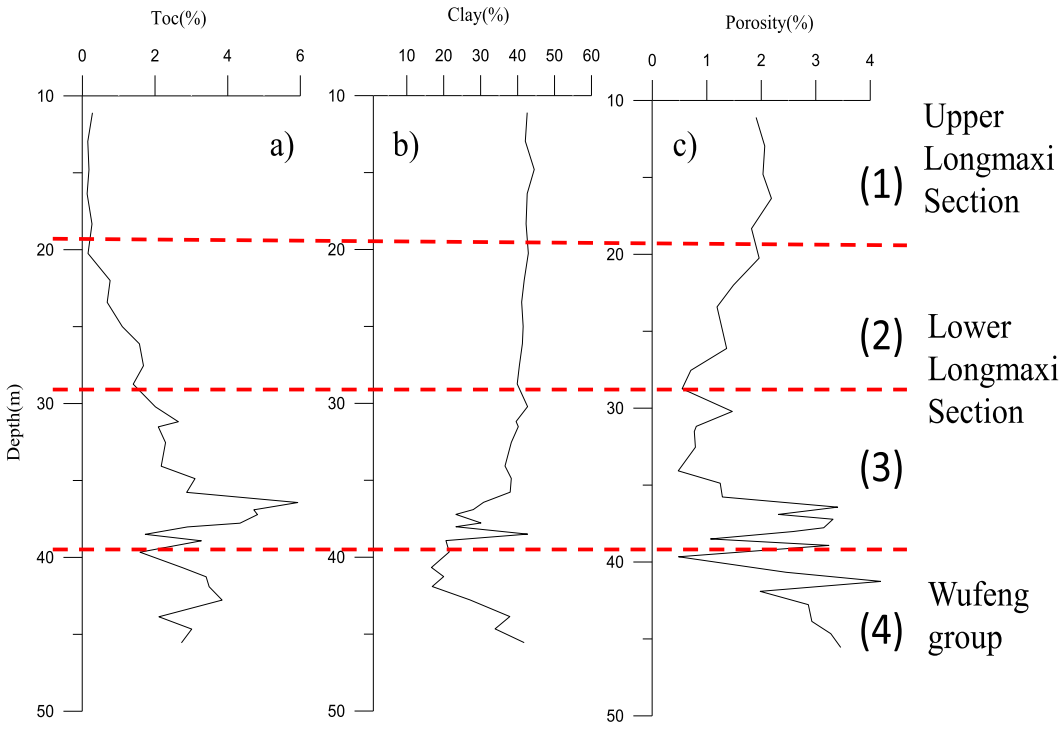

Fig. 3. Profile of TOC, clay content and porosity of shales in YH well.

4.2. FE-SEM imaging and pore types

According to the International Union of Pure and Applied Chemistry, nanometer-scaled pores have been classified into three categories: macropores (>50 nm), mesopores (2–50 nm), and micropores (<2 nm) (IUPAC, 1994). The FE-SEM technique is widely used to describe pore morphology (Chalmers et al., 2012a; Curtis et al., 2012; Tian et al., 2015; Wang et al., 2014) and to group nanopores based on pore location, either in the mineral matrix or organic matter (Loucks et al., 2012).

Intraparticle (intrap) pores are usually observed within mineral particles ranging from a ductile to rigid mineral matrix. For example, quartz contains intrap pores with diameters in the tens of nanometers (Fig. 4a). These pores are usually isolated and are possibly created by dissolution of unstable grains (Chalmers et al., 2012a; Wang et al., 2014). Interparticle (interp) pores created by flocculation (Slatt and O'Brien, 2011) are developed between the particles and crystals. Images of interp pores present along the edges of minerals and organic matter (OM)(Fig. 4). In clay platelets, interp pores between clay layers and intrap pores within them are usually accompanied by each other (Fig. 4a). Macropores associated with clays can also be produced by distortion of clay palettes during compaction (Fig. 4d). Pores within OM, which are regarded as significant within the pore network (Chalmers et al., 2012a; Curtis et al., 2012; Löhr et al., 2015; Milliken et al., 2013; Wang et al., 2014), are thought to be developed during maturation and expulsion of generated hydrocarbons (Chalmers and M., 2008; Chen and Xiao, 2014; Jarvie et al., 2007; Ross and Marc Bustin, 2009). More recently, however, this hypothesis has come into question because pores have also been found in immature shales (Löhr et al., 2015). Organic pores commonly distributed in the images of Fig. 4a–f vary in size from tens to hundreds of nanometers, though such measurements are limited by the resolution of FE-SEM. Besides, micro fractures resulted from shrinking or decompression effects (Chalmers et al., 2012a; Tian et al., 2015) can connect the nano-scaled pores in OM, clays and other grains.

In viewing FE-SEM images, geologists generally recognize minerals by their gray colour and regular shapes, and identify OMs by their black colour and irregular shapes. Moreover, some organic matter is mixed with clays to form an organo-clay complex, which has a dark gray colour (note c1, d1 and e1 areas in Fig. 4). It can be seen that more organic pores exist in the c1 area than in the c2 area. Previous researchers attribute the OM with poor pores (c2 area) to woody OM or different macerals (Curtis et al., 2012; Loucks et al., 2012). However, this study proposes that the compositions of OM may affect the development of organic pores. Thus, EDS analysis was conducted to identify the elemental compositions for selected areas in Fig. 4e and f. An organo-clay complex, formed by the mixing of OM and clay minerals, can be confirmed by the identification of Al, Si, O, and C elements (Fig. 5). However, because Al and Si may be present in either illite or chlorite, it is difficult to accurately quantify the content of these clay minerals in the organo-clay complex using the atomic proportions shown in Table 1. Thus, the relative content of silicon (Si) is chosen to qualitatively describe the total content of clay in the same image. Higher Si content is found in the e1 area (9.6%) than in the e3 area (5.3%). Correspondingly, larger organic pores can be seen in the e1 area compared to the e3 area. The situation is similar in Fig. 4f, that is, large organic pores are associated with a high Si content (6.3%) in the f2 area, where small organic pores are associated with low Si content (5.3%) in the f4 area. In general, larger organic pores are commonly developed in organo-clay complexes with high clay content than in those with low clay content.

Organic pores can form preferential flow paths in a continuous

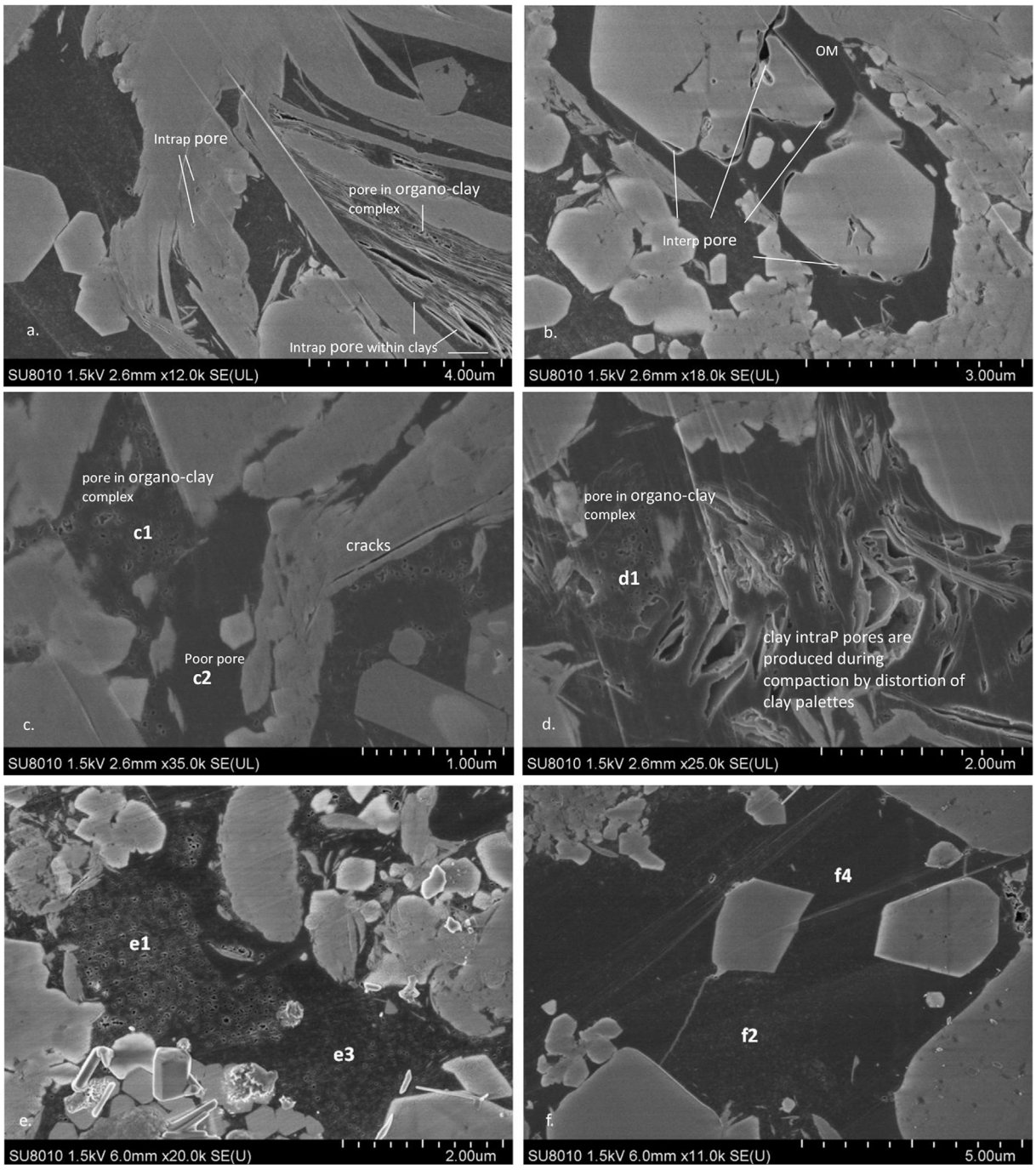

Fig. 4. FE-SEM images showing (a) intrap pores in brittle and clay minerals, (b) interp pores between quartz and OM, (d) clay interp pores produced by compaction, and (c–f) Organic pores in organo-clay complex (c–f).

organic framework and are thus significant features to consider in shale gas reservoir exploration and assessment (Loucks et al., 2012). Results from this research suggest that pore characteristics in organo-clay complexes play an even more important role than previously thought and that greater attention should be placed on pores in organo-clay complexes from this point forward.

4.3. Helium porosity and controlling factors

The helium porosity of the shale samples ranges from 0.48% to 4.2%, values slightly lower than those of American shales (Chalmers et al., 2012a; Ross and Marc Bustin, 2009). The shale samples are divided into two groups, one with high TOC (>2%) and the other one with low TOC values (<2%). A plot of TOC content versus helium porosity is shown in Fig. 6a. For samples with low TOC (<2%), porosity decreases with increasing TOC indicating that TOC is not the controlling factor. Given that large amounts of microporosity exist on the surface of and between layers of the clay platelets (Ross and Marc Bustin, 2009), it is assumed that clay content is correlated with porosity. Subsequently, a positive relationship between them is found (Fig. 6b), demonstrating that clay, particularly the illite fraction, significantly contributes to the porosity in samples with

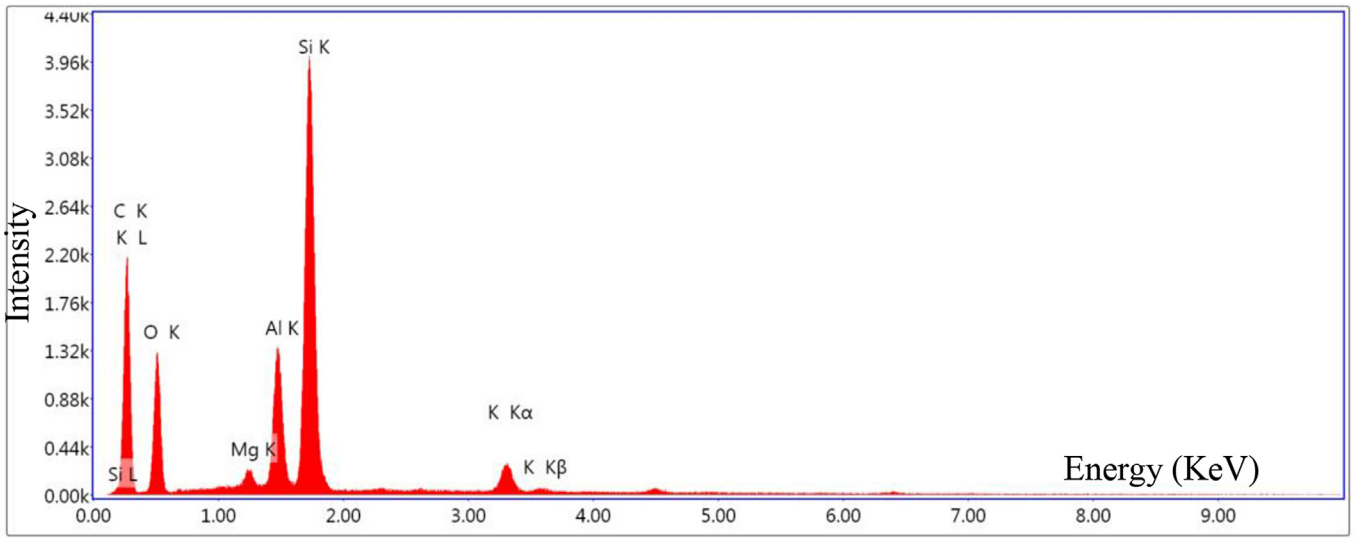

Fig. 5. EDS spectra for e1 area in Fig. 4.

Table 1
EDS results for e1, e3, f2, f4 areas in Fig. 4.

Element	Fig. 5e-Area 1	Fig. 5e-Area 3	Fig. 5f-Area 2	Fig. 5f-Area 4
	Atom(%)	Atom(%)	Atom(%)	Atom(%)
C	72.8	76.1	87.6	82.2
O	15.0	9.3	6.0	12.3
Mg	0	0.3	0	0
Al	1.3	1.4	0.1	0.16
Si	9.6	5.3	6.3	5.3
S	0.5	4.6	0	0
K	0.5	0.7	0	0
Fe	0.3	2.4	0	0

low TOC content (<2%). For successive organic-rich shales (TOC > 2%), the TOC and porosity data are dispersed and display a weak positive relationship, while there is no correlation between clay content and porosity. Therefore, TOC is considered a controlling factor for porosity in shales with high TOC content (>2%), while other factors (e.g. inorganic matrix) also influence porosity.

4.4. N_2 and CO_2 adsorption results

Six of the 34 adsorption/desorption isotherm curves of N_2 conducted at 77.35 K are selectively shown in Fig. 7. The amount of N_2 absorped at p/p_0 of about 0.995 varies from 18.4 cm^3/g to 50.8 cm^3/g for the 34 shales. The isotherms are classified as type IV isotherms, which are characterized by a type H3 hysteresis loop (Sing et al., 1985). Based on the shape of the hysteresis loop, slit-shaped pores may occur in these shales. Not surprisingly, FE-SEM observations demonstrate that bubble-, triangular-, and other irregularly-shaped pores were also found in this study, consistent with results for other shales in North American and China (Loucks et al., 2012; Milliken et al., 2013; Tian et al., 2015). The high adsorption of N_2 at low p/p_0 (<0.01) indicates the presence of micropores, while the continuous increase in adsorped N_2 with increasing relative pressure (up to the maximum of 0.995) is attributed to mesopores and macropores (Sing et al., 1985). The "forced closure" at a p/p_0 value of ~0.45 can be seen on the desorption branch for many N_2 isotherms. This closure is caused by the tensile strength effect, that is, the breaking of the hemispherical meniscus at a critical diameter of 4 nm (Groen et al., 2003). Meantime, the desorbed amount of N_2 at low relative pressure ($p/p_0 < 0.45$) is not equal to the adsorbed amount, which is attributed to swelling or adsorption in micropores (Gregg et al., 1967).

The total specific surface area of the 34 shale samples calculated from the BET equation (S_{BET}) ranges from 13.2 m^2/g to 26.9 m^2/g (Fig. 8). The vague positive relationship between TOC and total specific surface area implies that S_{BET} is not only controlled by organic matter content but is also likely related to variations in lithology or mineral composition. As seen in the supplementary file, the total surface area is dominated by the surface area of micropores (about 45–88% of S_{BET} for all samples).

Pore sizes associated with clay platelets range in the tens to hundreds of nanometers (Fig. 4a, c, d). Clay content is well correlated with both BJH surface area (S_{BJH}) and pore volume (V_{BJH}) as exhibited by the plots in Fig. 8a and b. This correlation suggests these pores, which includes those within or between clay platelets, interp pores between OM and clays, or organic pores in the organo-clay complex, are associated with clay minerals. Mesopores and macropores play an important role in clay minerals (Chalmers et al., 2012b; Ross and Marc Bustin, 2009; Wang et al., 2015); however, five samples from the Upper Longmaxi Formation are grouped separately from the others and below the trend line (Fig. 9). These samples all have relatively high proportions of chlorite, which has been reported to block the nanopores in shales (Bi et al., 2014; Li et al., 2015). The absence of interp pores between OM and clays, and organic pores in the organo-clay complex may be responsible for this phenomenon, given that these five samples are organic-poor and clay-rich. The plots in Fig. 9 clearly demonstrate that S_{BJH} and V_{BJH} are largely influenced by the clay fraction in Middle Yangtze region shales, although samples with high clay content but low TOC (<0.3%) have small BJH surface area and pore volume. This result suggests that 1.7–300 nm sized nanopores may be closely related to clay minerals (especially for illite)(Wang et al., 2015).

Six selected type I adsorption isotherms (Sing et al., 1985) for CO_2 are plotted in Fig. 10a. Maximum adsorption of CO_2 at a p/p_0 of approximately 0.03 varies from 0.95 to 2.93 cm^3/g. A positive relationship between TOC and maximum adsorption amount exists in these shales (Fig. 10 b), indicating a significant proportion of micropores is contained within organic matter (Wang et al., 2015). The DFT surface area (S_{DFT}) varies from 7.5 cm^2/g to 22.4 cm^2/g. Although TOC covers a wide range (0.13%–5.9%) in shales from the YH well, the surface area and pore volume of the micropores

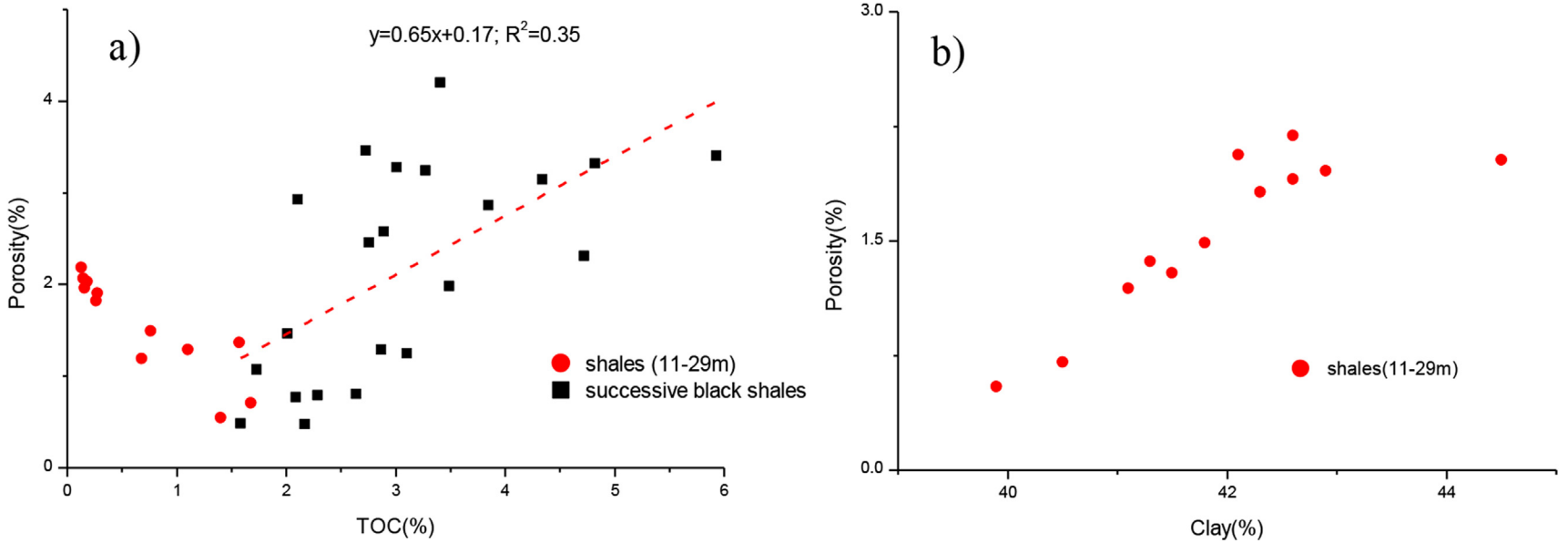

Fig. 6. (a) Correlations between TOC content and porosity for all samples; (b) Correlations between clay content with porosity for samples with low TOC content (<2%).

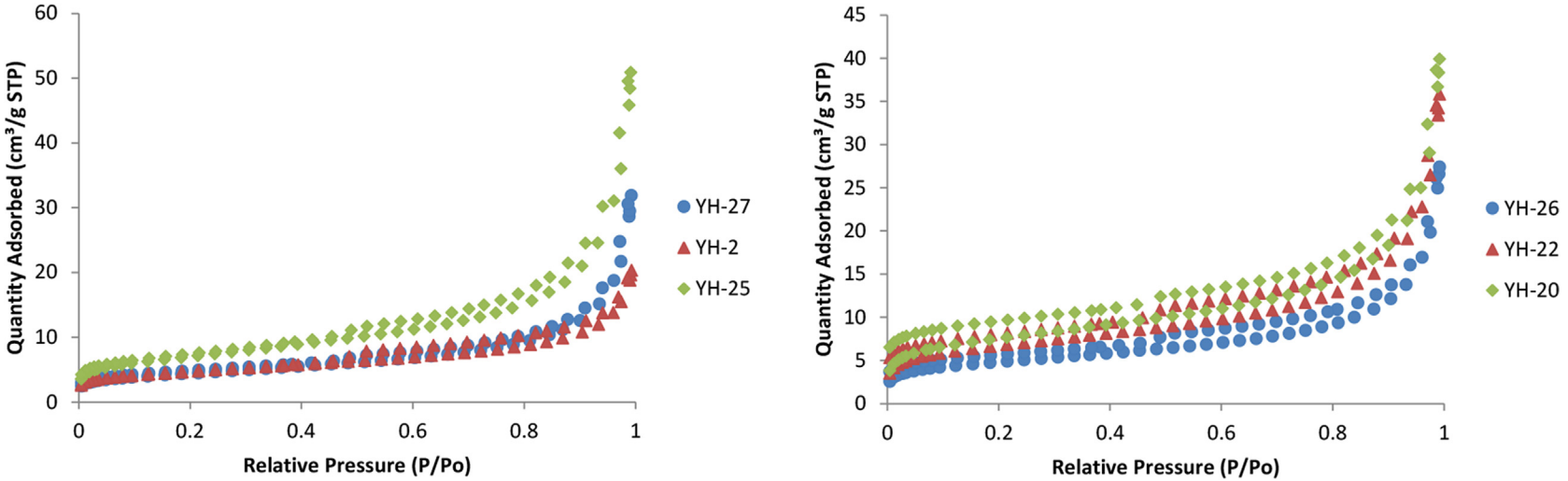

Fig. 7. Nitrogen gas adsorption and desorption isotherms for selected shales.

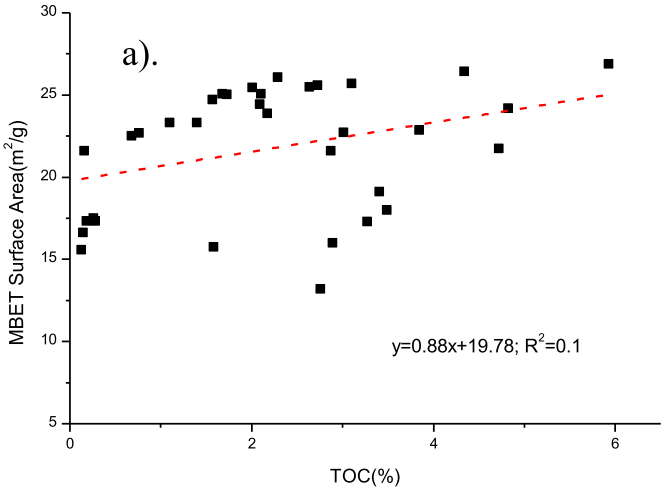

Fig. 8. Relationship between TOC content and BET surface area.

ate well with TOC content among all samples (Fig. 11). Moreover, evidence from the FE-SEM images demonstrates that, except for some tiny organic pores, most pore sizes are in the mesopore to macropore range (Fig. 4). Thus, the presence of micropores are limited to those in organic matter, consistent with results from small-angle neutron scattering and helium ion microscopy (King et al., 2015). The origin and development of micropores are usually attributed to kerogen thermal decomposition and generation of hydrocarbons (Chalmers and M., 2008; Jarvie et al., 2007; King et al., 2015; Ross and Marc Bustin, 2009).

4.5. Pore size distribution

Pore size distributions (PSD) of mesopores can be calculated by either the BJH or the DFT molecular model (Tian et al., 2013). However, the PSD calculated by the DFT model - developed from carbon slit-like pores (Dombrowski et al., 2000) - is the more accurate and preferred application for micropores and mesopores (Do and Do, 2003). Using the DFT model, a combination of the PSD of N_2 (1.7–300 nm) and CO_2 (<2 nm) adsorption data can be shown on a large scale (0.3–300 nm). Plots of dV/dw and dV/dlogw versus pore width (w) are frequently used to investigate PSD. The former plot illustrates the frequency of pores at specific pore widths. However, the latter is preferred in this study because it can assess the partial porosity of pores at any pore width (Tian et al., 2013; Wang et al., 2014).

The pore size distributions of shales collected from the YH well plotted in Fig. 12 are divided into four groups. The first group (e.g. YH-5, TOC = 0.26%) shows modes at approximately 0.4–0.7 nm, 1.0–1.7 nm, and 2.7–100 nm. The pore volume of these shales is mostly attributed to mesopores and macropores (1.0–1.7 nm, 2.7–100 nm) with little contribution from pores with widths larger than 100 nm. The second group (e.g. YH-30, TOC = 3.49%) shows modes at approximately 0.4–0.7 nm, 1.0–1.9 nm, 3.7–23.4 nm and 29.5–136 nm. The pore volume of these shales is also comprised of mesopores and macropores but with an absence of pores having widths around 2.7 nm. The third group (e.g. YH-28, TOC = 2.75%) shows modes at approximately 0.4–0.7 nm, 1.0–1.7 nm and 4.3–159 nm where the pore volume is mainly comprised of pores having widths of greater than 10 nm. Meantime, the plot of dV/dlogw versus pore width illustrates that pores which have widths greater than 100 nm are also developed. These macropores (>100 nm) may be related to the microfractures shown in FE-SEM images (Fig. 4 c). The TOC values for a majority of the 25 samples

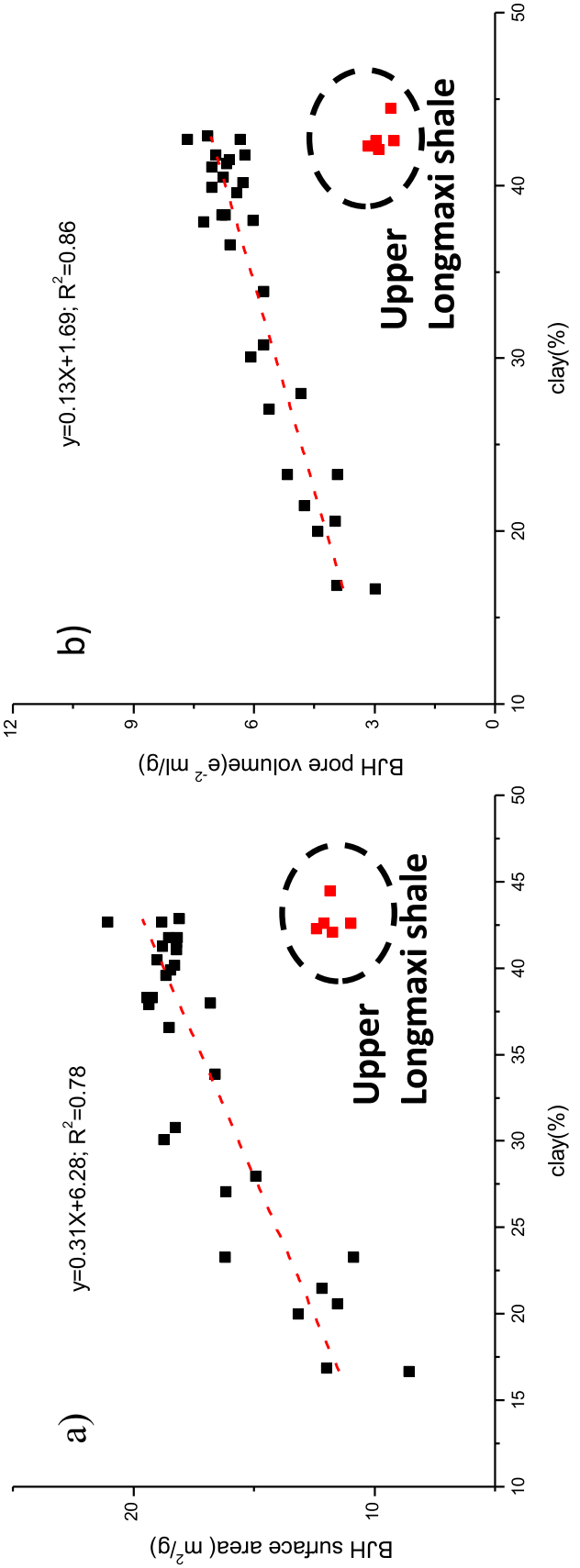

Fig. 9. Relationship between clay content and (a) BJH surface area and (b) pore volume.

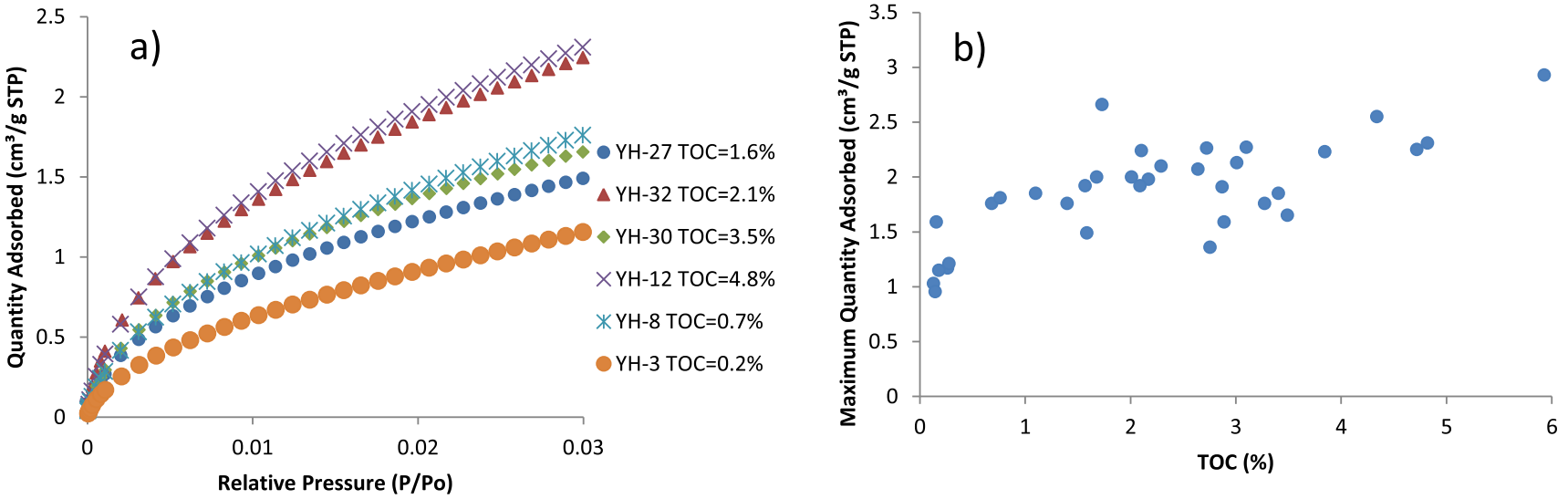

Fig. 10. (a) Isotherms of CO_2 adsorption and (b) Positive relationship between TOC content and the maximum amount of adsorbed CO_2.

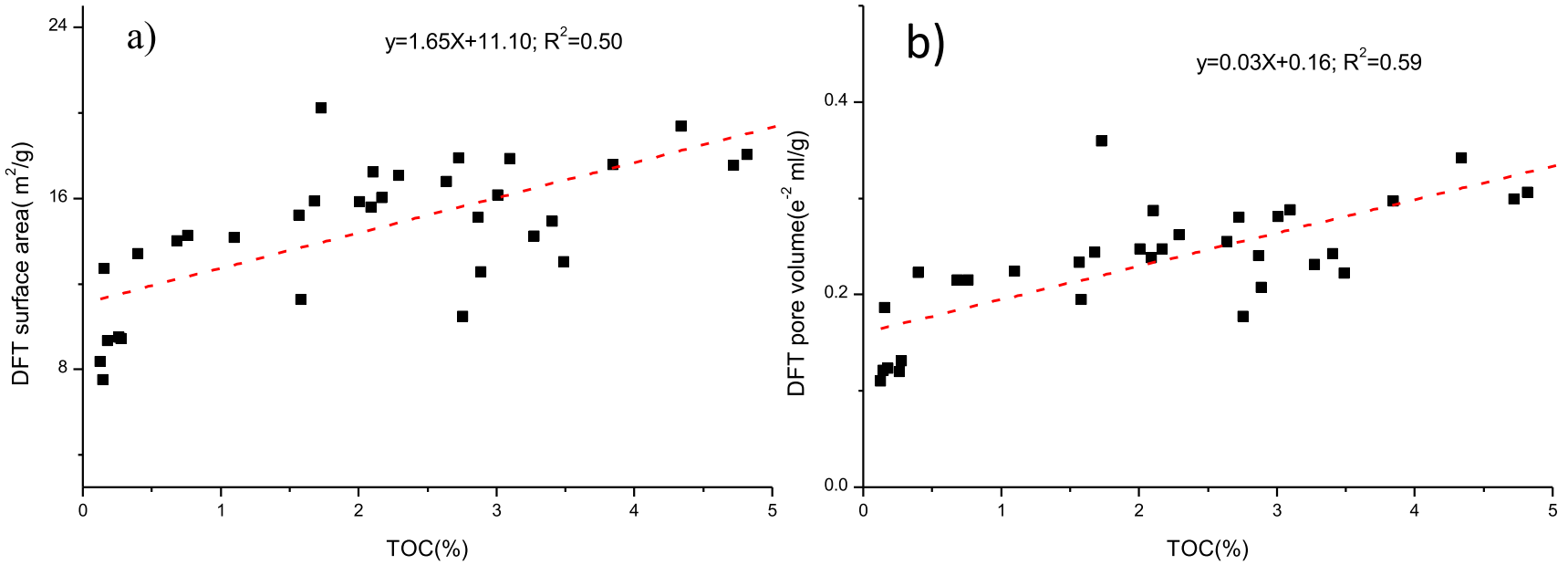

Fig. 11. Positive relationships between TOC content and (a) DFT surface area and (b) pore volume.

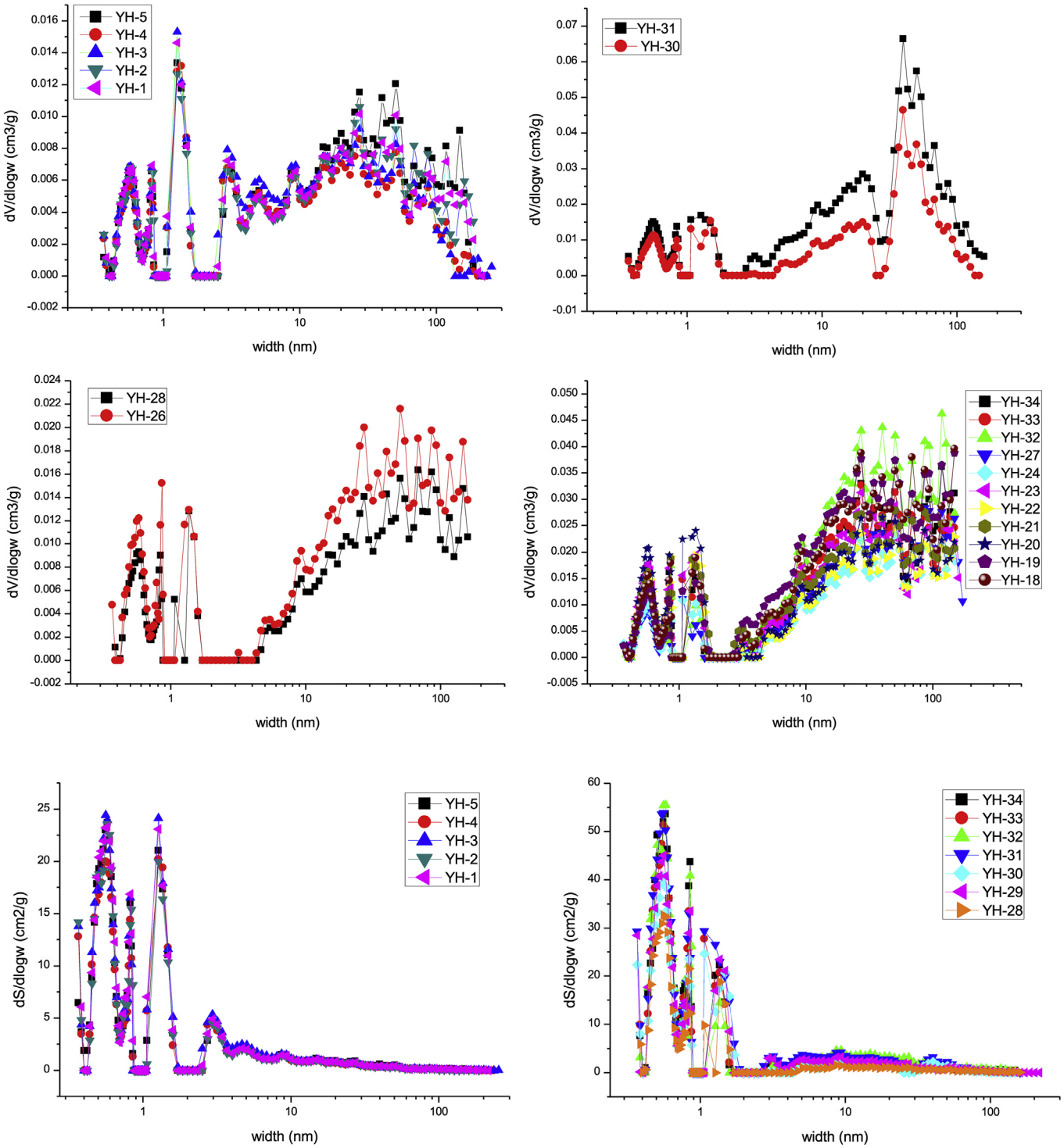

Fig. 12. Combination of PSD from N_2 and CO_2 gas adsorption.

in the fourth group are larger than 2%, close to those of the third group yet with higher relative proportions of large pores (>10 nm). Larger pores occupy a higher percentage of the total pore volume than small pores do (Tian et al., 2013) because the volume of a large pore is several times that of a small pore. For most of the organic-rich shales (TOC>2%) analyzed in this study, the larger mesopores and macropore, which provide effective storage space for free gas (Montgomery et al., 2005; Ross and Marc Bustin, 2009), contributed most to the total pore volume.

The plot of dS/dlogw versus pore width (w) in Fig. 12 depicts two groups of samples. The first group (YH-1 to YH-5, TOC< 0.3%) of samples is organic-poor and exhibits multiple modes of pore width in the ranges of 0.4–0.7 nm, 1–1.7 nm and 2.3–10 nm. The surface area in this group is comprised mainly of micropores (0.4–0.7 nm and 1–1.7 nm), consistent with results described for other shales in China (Tian et al., 2013; Wang et al., 2014) and North American (Chalmers et al., 2012a). Most of the 29 samples in the second group have TOC values greater than 2% and also exhibit multiple modes

with pore width in the ranges of 0.4–0.7 nm, 1–1.7 nm and 2.9–23 nm. As stated in previous studies, micropores contribute more to the total surface area (sorption site for methane) than mesopores, whereas macropores contribute the least (Chalmers et al., 2012a). Specifically, micropores with widths in the range of 0.4–0.7 nm contributed the most to total surface area in this research.

4.6. Impact of shale composition on pore structure

Organic matter and the mineral matrix have varying pore types, porosities, pore volumes and surface areas. Many researchers have investigated the relationship between shale composition and pore structure. A positive relationship between TOC and total porosity exists in samples with TOC values lower than 5.5%, while an inverse relationship occurs for samples with TOC values higher than 5.5% (Milliken et al., 2013). Organic pores have better connectivity than intrap pores (Loucks et al., 2012) and can form an effective pore system where shale gas flows dominantly (Ambrose et al., 2010; Curtis et al., 2010). In addition, inorganic material containing mesopores associated with the aluminosilicate fraction can influence porosity and PSD. Ross and Marc Bustin (2009) found that total porosities are larger in clay-rich shales compared to silica-rich shales (Ross and Marc Bustin, 2009). The OM/clay mineral intergranular pores are thought to be the primary spaces for gas storage in the Lower Cambrian Lujiaping Formation since these shales have been subjected to intense tectonic activities (Ma et al., 2015).

In this study, the nanopores in Lower Silurian and Upper Ordovician shales were found to be highly influenced by OM. This understanding can be confirmed by (1) the positive relationship which exists between TOC and porosity and (2) the absence of a relationship between clay content and porosity. As discussed in Section 4.4, micropores are only present in OM while mesopores and macropores are present in clay minerals. The PSD illustrates that the pore volume of these studied shales is mainly composed of nanopores with widths of more than 10 nm. Subsequently, it is easy to conclude that the nanopore network is primarily comprised of mesopores and macropores which are related to the clay fraction. However, this conclusion is incorrect because the basis of the problem involves the superficial nature of the positive correlation between clay content and V_{BJH}. Previous studies state that organic pores are the most abundant pore type and constitute as much as 71.5% of all pores in the Longmaxi Shale (Jiao et al., 2014), and large quantities of such pores are found in organo-clay complexes (Fig. 4). Organic pores may be collectively associated with clay minerals and OM. In summary, the TOC content is the shale characteristic most closely associated with the development of nanopores in the Longmaxi Shale, followed by clay content.

4.7. Mechanism of shale gas storage and shale gas potential in the Middle Yangtze region

Shale gas exists as both free and adsorbed gases in mature shale (Hao and Zou, 2013; Zhang et al., 2012). The free gas, present in microfractures and macropores, is controlled by porosity and gas saturation (Pan et al., 2016). For certain shales, the amount of adsorbed gas located in micropores and mesopores is determined by geologically-imposed pressure and temperature conditions (Hao and Zou, 2013; Hao et al., 2013). The absorbed gas alone cannot keep sufficient gas in-situ to be a commercial shale gas field (Hao et al., 2013). Thus, a closed shale gas system is required to contain the free gas in reservoirs.

In this study, low TOC values (<2%) and low porosity (<1%) characterize the middle of the Longmaxi Formation at a depth of 27–34 m (Fig. 3c). Although the thick shales with low TOC may not generate much shale gas, their low porosity hinders the upward immigration of gas from the bottom. These low-porosity shales probably serve as a cap to keep gas remaining within the organic-rich Longmaxi Shale.

The shales with TOC >2% have a total porosity of 1–4.2% and a BET surface area of 13–27 m^2/g. The storage capacity for both free and adsorbed gas increases with TOC. The gas-in-place (GIP) models raised by Pan et al. (2016) states that an effective shale gas reservoir typically has a burial depth of greater than 1000 m. That is, the total gas content decreases rapidly due to the reduction in the storage capacity of both free and adsorbed gas at depths of less than 1000 m (Pan et al., 2016). Given that the Longmaxi Shale is situated under well preserved conditions and at a depth of greater than 1000 m in the North part and west part of Middle Yangtze region, it provides a suitable target for shale gas exploration. In addition, two successful cases exist in which shale gas collected by desorption jar from the Laidi 1 well (west part of this region) and the Zidi 1 well (north part of this region) was successfully ignited. These activities, together with the encouraging pore characteristics of the Longmaxi shales examined in this study, indicate a high potential for shale gas exploration in this region.

5. Conclusions

Thirty-four shale samples collected from the Upper Ordovician and Lower Silurian formations were analyzed to determine their nanopore characteristics. The most significant outcomes are as follows:

1. Samples extracted from the Wufeng Shale and from the bottom of the Longmaxi Shale are rich in organic matter, with TOC ranging from 1.6% to 5.9% and clay content ranging from 16.7% to 42.7%. The total porosity for successive black shales varies from 0.5% to 4.2%, with BET surface area ranging from 13.2 to 26.9 m^2/g, both of which are weakly positively correlated with TOC values.
2. The FE-SEM images and EDS results indicate that numerous organic pores exist in organo-clay complexes. Larger organic pores are usually developed in organo-complexes with higher clay content compared to those with lower clay content.
3. The surface area and pore volume of mesopores and macropores both have a positive relationship with clay content, indicating a significant contribution from clay minerals to these pores. Most pores are commonly found in the mesopore to macropore scale range, while micropores can be limited to the contribution from OM. This assumption is confirmed by the good correlation between S_{DFT} (or P_{DFT}) and TOC.
4. The DFT-derived PSD illustrate that total pore volume is mainly comprised of pores having widths greater than 10 nm, and surface areas is mostly derived from pores having widths of 0.4–0.7 nm.
5. The shales in the middle of Longmaxi Formation have low porosity and probably cap the shale gas generated from the organic-rich Longmaxi shales at the bottom. As with the Laidi 1 and Zidi 1 wells, further exploration of shale gas in the Middle Yangtze region should focus on the Longmaxi shale, which is well preserved and deeply buried (e.g. > 1000 m).

Acknowledgments

This study was supported by a special program of Chinese Academy of Science (XDB10010504), the National Science Foundation of China (41602130, 41572125), the Nation Key Basic Research Program of China (973 Program: 2012CB214706) and the Natural Science Foundation of Guangdong Province (2016A030310116). Special acknowledgements are given to Prof. Juanxuan Fan and Dr. Zongyuan Sun for assistance in sample

collection. Editor-in-Chief Massimo Zecchin and the guest editor are thanked for their patient editorial work. The two anonymous reviewers are thanked for their instructive comments and suggestions that significantly improve this manuscript. This is contribution NO. IS-2324 from GIGCAS.

Appendix A. Supplementary data

Supplementary data related to this article can be found at http://dx.doi.org/10.1016/j.marpetgeo.2016.12.015.

References

Ambrose, R.J., Hartman, R.C., Diaz Campos, M., Akkutlu, I.Y., Sondergeld, C., 2010. New pore-scale considerations for shale gas in place calculations. Soc. Pet. Eng.
Barrett, E.P., Joyner, L.G., Halenda, P.P., 1951. The determination of pore volume and area distributions in porous substances. I. Computations from nitrogen isotherms. J. Am. Chem. Soc. 73, 373–380.
Bernard, S., Horsfield, B., Schulz, H.-M., Wirth, R., Schreiber, A., Sherwood, N., 2012. Geochemical evolution of organic-rich shales with increasing maturity: a STXM and TEM study of the Posidonia Shale (Lower Toarcian, northern Germany). Mar. Petroleum Geol. 31, 70–89.
Bi, H., Jiang, Z., Li, P., Li, Z., Tang, X., Zhang, D., Xu, Y., 2014. Shale reservoir characteristics and its influence on gas content of Wufeng-Longmaxi Formation in the southeastern Chongqing. Nat. Gas. Geosicence 25, 1275–1283.
Brunauer, S., Emmett, P.H., Teller, E., 1938. Adsorption of gases in multimolecular layers. J. Am. Chem. Soc. 60, 309–319.
Cao, T., Song, Z., Wang, S., Cao, X., Li, Y., Xia, J., 2015. Characterizing the pore structure in the silurian and permian shales of the Sichuan Basin, China. Mar. Petroleum Geol. 61, 140–150.
Chalmers, G.R.L., M., B.R., 2008. Lower Cretaceous gas shales in northeastern British Columbia, Part I: geological controls on methane sorption capacity. Bull. Can. petroleum Geol. 56, 1–21.
Chalmers, G.R., Bustin, R.M., Power, I.M., 2012a. Characterization of gas shale pore systems by porosimetry, pycnometry, surface area, and field emission scanning electron microscopy/transmission electron microscopy image analyses: examples from the Barnett, Woodford, Haynesville, Marcellus, and Doig units. AAPG Bull. 96, 1099–1119.
Chalmers, G.R.L., Ross, D.J.K., Bustin, R.M., 2012b. Geological controls on matrix permeability of devonian gas shales in the horn river and liard basins, northeastern british Columbia, Canada. Int. J. Coal Geol. 103, 120–131.
Chen, J., Xiao, X., 2014. Evolution of nanoporosity in organic-rich shales during thermal maturation. Fuel 129, 173–181.
Chen, Y., Wei, L., Mastalerz, M., Schimmelmann, A., 2015. The effect of analytical particle size on gas adsorption porosimetry of shale. Int. J. Coal Geol. 138, 103–112.
Curtis, J.B., 2002. Fractured shale-gas systems. AAPG Bull. 86, 1921–1938.
Curtis, M.E., Ambrose, R.J., Sondergeld, C.H., 2010. Structural Characterization of Gas Shales on the Micro-and Nano-scales, Canadian Unconventional Resources and International Petroleum Conference. Society of Petroleum Engineers.
Curtis, M.E., Cardott, B.J., Sondergeld, C.H., Rai, C.S., 2012. Development of organic porosity in the Woodford Shale with increasing thermal maturity. Int. J. Coal Geol. 103, 26–31.
De Silva, P.N.K., Simons, S.J.R., Stevens, P., Philip, L.M., 2015. A comparison of North American shale plays with emerging non-marine shale plays in Australia. Mar. Petroleum Geol. 67, 16–29.
Do, D.D., Do, H.D., 2003. Pore characterization of carbonaceous materials by DFT and GCMC simulations: a review. Adsorpt. Sci. Technol. 21, 389–423.
Dombrowski, R.J., Hyduke, D.R., Lastoskie, C.M., 2000. Pore size analysis of activated carbons from argon and nitrogen porosimetry using density functional theory. Langmuir 16, 5041–5050.
Eseme, E., Littke, R., Krooss, B.M., 2006. Factors controlling the thermo-mechanical deformation of oil shales: implications for compaction of mudstones and exploitation. Mar. Petroleum Geol. 23, 715–734.
Ghosal, R., Smith, D., 1996. Micropore characterization using the Dubinin-Astakhov equation to analyze high pressure CO2 (273 K) adsorption data. J. Porous Mater 3, 247–255.
Gregg, S.J., Sing, K.S.W., W., S.H., 1967. Adsorption surface area and porosity. J. Electrochem. Soc. 114, 279C, 279C.
Groen, J.C., Peffer, L.A.A., Pérez-Ramírez, J., 2003. Pore size determination in modified micro- and mesoporous materials. Pitfalls and limitations in gas adsorption data analysis. Microporous Mesoporous Mater. 60, 1–17.
Guo, T., Zhang, H., 2014. Formation and enrichment mode of Jiaoshiba shale gas field, Sichuan Basin. Petroleum Explor. Dev. 41, 31–40.
Hao, F., Zou, H., 2013. Cause of shale gas geochemical anomalies and mechanisms for gas enrichment and depletion in high-maturity shales. Mar. Petroleum Geol. 44, 1–12.
Hao, F., Zou, H., Lu, Y., 2013. Mechanisms of shale gas storage: implications for shale gas exploration in China. AAPG Bull. 97, 1325–1346.
Jarvie, D.M., Hill, R.J., Ruble, T.E., Pollastro, R.M., 2007. Unconventional shale-gas systems: the Mississippian Barnett Shale of north-central Texas as one model for thermogenic shale-gas assessment. AAPG Bull. 91, 475–499.
Jiao, K., Yao, S., Liu, C., Gao, Y., Wu, H., Li, M., Tang, Z., 2014. The characterization and quantitative analysis of nanopores in unconventional gas reservoirs utilizing FESEM–FIB and image processing: an example from the lower Silurian Longmaxi Shale, upper Yangtze region, China. Int. J. Coal Geol. 128–129, 1–11.
King Jr., H.E., Eberle, A.P., Walters, C.C., Kliewer, C.E., Ertas, D., Huynh, C., 2015. Pore architecture and connectivity in gas shale. Energy & Fuels 29, 1375–1390.
Löhr, S.C., Baruch, E.T., Hall, P.A., Kennedy, M.J., 2015. Is organic pore development in gas shales influenced by the primary porosity and structure of thermally immature organic matter? Org. Geochem. 87, 119–132.
Li, H., Liu, D., Peng, P.a., Wang, Q., 2015. Tectonic impact on reservoir character of Chongqing and its neighbor area. Nat. Gas. Geosicence 26, 1705–1711.
Loucks, R.G., Reed, R.M., Ruppel, S.C., Hammes, U., 2012. Spectrum of pore types and networks in mudrocks and a descriptive classification for matrix-related mudrock pores. AAPG Bull. 96, 1071–1098.
Loucks, R.G., Ruppel, S.C., 2007. Mississippian barnett shale: lithofacies and depositional setting of a deep-water shale-gas succession in the Fort Worth basin, Texas. AAPG Bull. 91, 579–601.
Ma, Y., Zhong, N., Li, D., Pan, Z., Cheng, L., Liu, K., 2015. Organic matter/clay mineral intergranular pores in the Lower Cambrian Lujiaping Shale in the north-eastern part of the upper Yangtze area, China: a possible microscopic mechanism for gas preservation. Int. J. Coal Geol. 137, 38–54.
Mastalerz, M., He, L., Melnichenko, Y.B., Rupp, J.A., 2012. Porosity of coal and shale: insights from gas adsorption and SANS/USANS techniques. Energy & Fuels 26, 5109–5120.
Milliken, K.L., Esch, W.L., Reed, R.M., Zhang, T., 2012. Grain assemblages and strong diagenetic overprinting in siliceous mudrocks, barnett shale (mississippian), Fort Worth basin, Texas. AAPG Bull. 96, 1553–1578.
Milliken, K.L., Rudnicki, M., Awwiller, D.N., Zhang, T., 2013. Organic matter–hosted pore system, Marcellus Formation (Devonian), Pennsylvania. AAPG Bull. 97, 177–200.
Montgomery, S.L., Jarvie, D.M., Bowker, K.A., Pollastro, R.M., 2005. Mississippian Barnett Shale, Fort Worth basin, north-central Texas: gas-shale play with multitrillion cubic foot potential. AAPG Bull. 89, 155–175.
Pan, L., Xiao, X., Tian, H., Zhou, Q., Cheng, P., 2016. Geological models of gas in place of the Longmaxi shale in southeast Chongqing, south China. Mar. Petroleum Geol. 73, 433–444.
Qiu, X., Yang, B., Hu, M., 2013. Characteristics of shale reservoirs and gas content of Wufeng-Longmaxi formation in the Middle Yangtze Region. Nat. Gas. Geosicence 24, 1274–1283.
Ross, D.J.K., Marc Bustin, R., 2009. The importance of shale composition and pore structure upon gas storage potential of shale gas reservoirs. Mar. Petroleum Geol. 26, 916–927.
Ruppert, L.F., Sakurovs, R., Blach, T.P., He, L., Melnichenko, Y.B., Mildner, D.F.R., Alcantar-Lopez, L., 2013. A USANS/SANS study of the accessibility of pores in the barnett shale to methane and water. Energy & Fuels 27, 772–779.
Sing, K.S.W., Everett, D.H., Haul, R.A.W., Moscou, L., Pierotti, R.A., Rouquerol, J., Siemienewska, T., 1985. Reporting physisorption data for gas/solid systems with special reference to the determination of surface area and porosity. Pure Appl. Chem. 57, 603–619.
Slatt, R.M., O'Brien, N.R., 2011. Pore types in the Barnett and Woodford gas shales: contribution to understanding gas storage and migration pathways in fine-grained rocks. AAPG Bull. 95, 2017–2030.
Tian, H., Pan, L., Xiao, X., Wilkins, R.W.T., Meng, Z., Huang, B., 2013. A preliminary study on the pore characterization of Lower Silurian black shales in the Chuandong Thrust Fold Belt, southwestern China using low pressure N2 adsorption and FE-SEM methods. Mar. Petroleum Geol. 48, 8–19.
Tian, H., Pan, L., Zhang, T., Xiao, X., Meng, Z., Huang, B., 2015. Pore characterization of organic-rich lower Cambrian shales in Qiannan depression of Guizhou province, southwestern China. Mar. Petroleum Geol. 62, 28–43.
Wang, Q., Shen, C., Chen, Q., Zhang, L., Lu, H., 2015. Pore characteristics and gas released by Crush methods of Wufeng-longmaxi shale in the northwest of Hubei province, China. Acta Geol. Sin. - Engl. Ed. 89, 93–96.
Wang, Y., Zhu, Y., Chen, S., Li, W., 2014. Characteristics of the nanoscale pore structure in northwestern hunan shale gas reservoirs using field emission scanning electron microscopy, high-pressure mercury intrusion, and gas adsorption. Energy & Fuels 28, 945–955.
Writing group for Petroleum Geology in Sichuan area, 1989. Petroleum Geology of China. Petroleum Industry Press, Beijing.
Zhang, T., Ellis, G.S., Ruppel, S.C., Milliken, K., Yang, R., 2012. Effect of organic-matter type and thermal maturity on methane adsorption in shale-gas systems. Org. Geochem. 47, 120–131.
Zou, C., Dong, D., Wang, S., Li, J., Li, X., Wang, Y., Li, D., Cheng, K., 2010. Geological characteristics and resource potential of shale gas in China. Petroleum Explor. Dev. 37, 641–653.